

Air entrainment and gas transfer processes in wave breaking events

Simone Di Giorgio^{1,2}, Sergio Pirozzoli³, and Alessandro Iafrati¹

¹ *Institute of Marine engineering - CNR - Rome, Italy*

² *Institute of Fluid Mechanics and Heat Transfer - TU-Wien, Austria*

³ *Department of Mechanics and Aerospace Engineering - Sapienza Univ. Rome, Italy*

(Dated: December 31, 2024)

We investigate gas transfer processes occurring at the air-water interface of progressive water waves using high-fidelity numerical simulations. Waves with varying initial steepness, including regular wave patterns, mild spilling and intense plunging breakers are examined. A multiphase solver is employed to model gas flux and diffusion processes enabling precise estimation of the air-water interface area and gas transfer velocity, achieving an accuracy unattainable in experiments. We reveal that the volume of gas transferred across the air-water interface increases significantly with the amount of air entrained due to wave breaking, peak values in the gas transfer velocity being concurrent with peaks in energy dissipation rate and air entrainment. Furthermore, the gas transfer velocity is observed to scale approximately as the one-fourth power of the energy dissipation rate, consistent with previous theoretical predictions. We anticipate that the present findings can help reduce the substantial uncertainty associated with parameterizing fundamental natural processes, such as CO₂ absorption by the oceans.

Gas exchange processes at the air-sea interface play a crucial role in regulating the climate and sustaining both human and marine life. A significant portion of anthropogenic carbon dioxide is absorbed by the ocean [1, 2], which, in turn, releases nearly half of the oxygen we breathe through the photosynthesis of marine flora in the sunlit upper ocean layer. For low-solubility gases such as oxygen, mass transfer is governed by molecular diffusion and turbulence within a very thin layer on the water side [3, 4]. Although the original motivation for the study stems from the exchange processes at the ocean surface, the gas transfer across a gas-liquid interface is of great interest in other contexts such as chemical, food and pharmaceutical industries where bubble columns are often used in chemical reactors [5].

Despite its importance, this process remains poorly understood [6]. Most studies have focused on correlating gas transfer velocity with wind speed (e.g., [7]), yet the underlying mechanisms driving gas exchange processes are not fully elucidated. One of the reasons is that laboratory measurements are extremely challenging as concentration fluctuations should be measured at depths of at most hundreds of micrometers to have direct relevance to air-water gas transfer [8], hence most investigations pertain to unbroken air-sea interfaces (e.g. [9, 10]). Despite the clear evidence that bubbles generated from wave breaking, with associated turbulence and energy dissipation, enhance significantly air-sea exchanges especially for poorly soluble gases, the parameterization of their effect is grossly inaccurate [11].

The gas transfer velocity is often expressed in terms of the near-surface turbulent dissipation rate (e.g., [12, 13]). Since air entrainment and bubble fragmentation are known to significantly promote energy dissipation [14], a similar effect on gas transfer is expected. The effect of air bubbles on mass diffusion involves two distinct cases:

smaller bubbles that lack sufficient buoyancy to rise and gradually dissolve into the water, and larger bubbles that dissolve partially while ascending and eventually burst at the free surface [15]. Measurements of the gas transfer velocity under breaking waves, induced via modulational instability with and without overlying wind, were conducted by [16]. The authors proposed that a Reynolds number, based on the breaker height and the mean orbital velocity of the breaking wave, is a relevant parameter. While it is anticipated that these parameters influence the bubble injection rate [14], no direct experimental evidence was provided. Additionally, in those experiments, the gas concentration was measured only before and after breaking, leaving the temporal evolution of the local concentration unobserved.

The significant progress of multiphase flow numerical solvers in the last fifteen years along with recent introduction of numerical methods to model gas transfer processes across gas-liquid interfaces [5, 17], have made it possible to investigate numerically the bubble-mediated contribution to the gas transfer. An attempt in this direction was made by [18], who studied the dissolved gas concentration in a two-dimensional breaking wave, with a somewhat unrealistic air-water density ratio of 10^{-2} . However, no quantitative data about gas transfer at the interface was provided.

In order to investigate gas transfer processes taking place during the breaking of free-surface waves and to identify the significance of air entrainment, herein we numerically simulate the time evolution of a third-order Stokes' wave [18–20], for various initial steepness, yielding a regular wave pattern, mild spilling breaking, and intense plunging breaking with substantial air entrainment. The flow is assumed to be three-dimensional and periodic along the streamwise (x) and spanwise (z) directions, y being the vertical axis. We solve the Navier-Stokes for an

incompressible fluid with variable fluid properties across the air-water interface, which we model after a geometric Volume-of-Fluid method [21]. A detailed description of the solver is provided in [20, 22].

The baseline multiphase solver is here augmented with a model to account for gas diffusion, whereby the time evolution of the gas concentration $c_{w/a}$ in water (w) and air (a) is determined by solving [23, 24]

$$\frac{\partial c_{w/a}}{\partial t} + \nabla \cdot (\mathbf{u}c_{w/a}) = -\nabla \cdot (\mathbf{J}_{w/a}),$$

where \mathbf{u} is the local fluid velocity, and $\mathbf{J}_{w/a}$ is the mass flux vector. The standard assumption of continuous chemical potentials at the air-water interface leads to Henry's law [25], expressed as

$$c_w = \alpha c_a,$$

where α is the solubility constant [26], assumed constant in this study. We use the water fraction (χ) to evaluate the local gas concentration as a weighted average of the values in air and water. Similarly, the local diffusivity coefficient is evaluated as a harmonic mean [27]. These formulations lead to the nondimensional form of the concentration equation,

$$\frac{\partial c}{\partial t} + \nabla \cdot (\mathbf{u}c) = \frac{1}{ReSc} \nabla \cdot \left(D \nabla c - D \left(\frac{c(\alpha - 1)}{\alpha\chi + (1 - \chi)} \right) \nabla \chi \right).$$

The convective term in the above equation is discretized with an upwind-biased TVD scheme [28].

A third-order wave is considered as initial condition [19, 20, 29], whose profile is specified as

$$\eta(x, z) = \frac{\epsilon}{2\pi} \left(\cos(kx') + \frac{\epsilon}{2} \cos(2kx') + \frac{3\epsilon^2}{8} \cos(3kx') \right),$$

where the wavelength λ is hereafter assumed to be the reference length, $k = 2\pi/\lambda$ is the fundamental wavenumber, $\epsilon = ak$ is the initial wave steepness, and $x' \approx x$, unless small random perturbation [20]. From wave theory, assuming $U_R = (g\lambda)^{1/2}$ as reference velocity and $T_R = (\lambda/g)^{1/2}$ as reference time, the nondimensional period of the fundamental wave component is $T_p = (2\pi)^{1/2}$. No-slip boundary conditions are enforced at the top and bottom boundaries. The initial velocity in the water domain ($y < \eta(x, z)$) is determined from second-order potential flow theory, whereas the air side is assumed at rest. The gas is initially assumed to be at the saturation point in the air domain and absent in the water domain, as shown in the top left panel of Fig. 1.

The energy content in water (E_w) is evaluated as the sum of the kinetic and potential contributions, as follows

$$E_w(t) = \int_{V_w} \rho \left(\frac{|\mathbf{u}|^2}{2} + gy \right) dV - E_{p0}, \quad (1)$$

where E_{p0} is the potential energy of the fluid at rest.

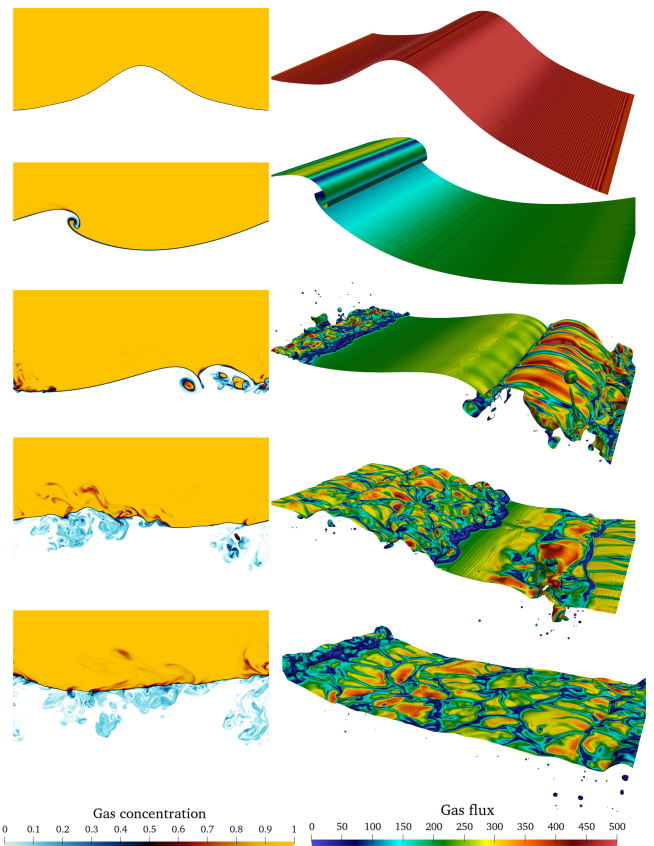


FIG. 1. Time sequence of gas concentration in a $x - y$ slice (left) and gas flux normal to the air-water interface (right). The data refer to the flow case with $\epsilon = 0.50$, $Re = 40,000$. From top to bottom $t/T_p = 0, 0.50, 1.00, 1.50, 2.00$.

The numerical simulations are carried out for Weber number $We = (\rho_w U_R^2 \lambda) / \sigma = 12,000$, with σ the surface tension coefficient, which corresponds to waves with about 30 cm fundamental wavelength. At such scale, the Reynolds number $Re = (\rho_w U_R \lambda) / \mu_w$ would be about 500,000, too high for all the scales to be fully resolved. Hence, numerical simulations are carried out at reduced Reynolds numbers $Re = 10,000$ and $Re = 40,000$, which correspond to fundamental wavelengths of 2.17 cm and 5.46 cm, respectively. Three values of the initial steepness are considered, $\epsilon = 0.25, 0.37$ and 0.50 , which lead, respectively, to a regular wave pattern, mild spilling breaking with small air entrainment, and intensive wave breaking with large air entrainment. The computational domain is one fundamental wavelength long, two wavelengths tall and half wavelength wide. It is discretized by using $N_x = 1152$, $N_z = 576$, $N_y = 768$ collocation points, the latter being clustered towards the still water level ($y = 0$). Assuming $\lambda = 30$ cm, the resulting grid size in the well-resolved zone is 0.26 mm. As for the dissolving gas, we assume the Schmidt number in water to be $Sc_w = \mu_w / (\rho_w D_w) = 4$, the diffusivity ratio to be $D_a / D_w = 100$, and the solubility constant to be $\alpha = 0.33$. The total amount of gas in air (q_a) and water

(q_w) can be determined from integration,

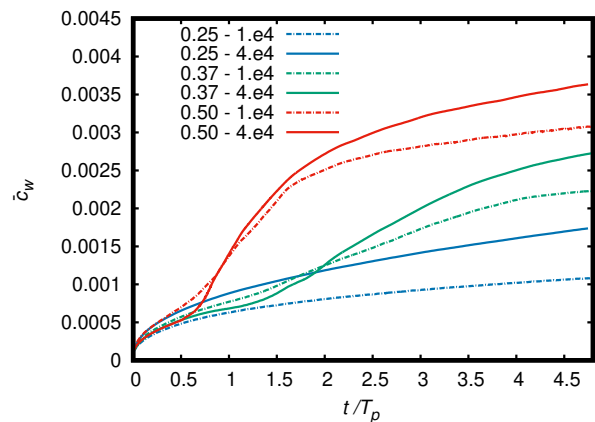
$$q_{a,w} = \int_{V_{a,w}} c(x, y, z) dV, \quad (2)$$

where $V_{a,w}$ is the volume occupied by the two phases. Mean concentrations of gas in air and water can then be defined as $\bar{c}_{a,w} = q_{a,w}/V_{a,w}$.

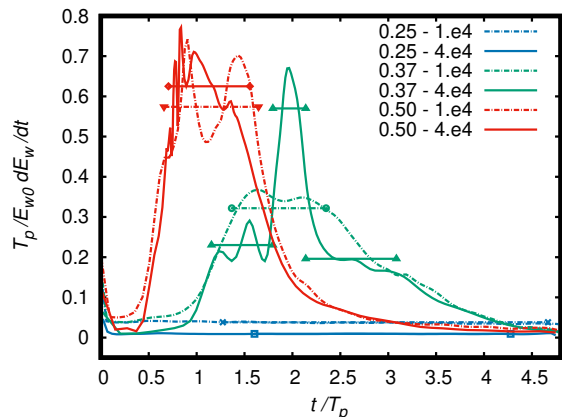
In Fig. 1, we present visualizations of the gas concentration and flux normal to the air-water interface at various stages of wave evolution for the case $\epsilon = 0.50$, $Re = 40,000$, which results in maximum gas transfer. The abrupt jump in gas concentration imposed as the initial condition causes a high gas flux through the interface at the start of the simulation, as shown in the top-right panel. This spurious transient is completed before the onset of breaking ($t/T_p \approx 0.5$). The sequence clearly illustrates that, during the early stages of the breaking process, gas transfer predominantly occurs across the air-water interface, with gas becoming trapped in air bubbles entrained in the water. At later stages, the entrapped gas diffuses into the water domain, accompanied by a corresponding decrease in concentration in the air domain.

To quantify the gas transfer process, Fig. 2 shows the mean gas concentration in water and the energy dissipation rate as functions of time. The gas concentration exhibits an initial transient lasting about half a wave period, which is similar for all cases. This phase is characterized by intense gas transfer across the air-water interface, driven by the artificial start-up, followed by a milder growth phase with a typical time scale associated with the wave orbital velocity. For the flow cases with $\epsilon = 0.25$, featuring a regular wave pattern, the growth rate of the mean gas concentration in water progressively decreases with time. In contrast, for the flow cases with $\epsilon = 0.50$, a sudden increase in the mean gas concentration is observed starting at about half a wave period. This increase coincides with the sharp rise in the energy dissipation rate, as shown in Fig. 2b, marking the onset of the plunging breaking event. Intense gas transfer persists up to $t \approx 2T_p$, after which the mass transfer rate returns to values similar to the non-breaking cases. In milder spilling breaking cases, breaking begins shortly before $t = T_p$, as evidenced by the increase in both gas transfer and energy dissipation rates. In these cases, the breaking process lasts longer, resulting in a gas transfer rate significantly lower than that in the plunging breaking cases. The rate approaches the non-breaking value around $t \simeq 4T_p$.

The results reported in Fig. 1 clearly convey that air entrainment plays an important role in the gas exchange process, as also observed by several previous authors [30, 31], and as pointed out in recent reviews of the subject [6, 7]. Our high-fidelity numerical model enables to make these qualitative statement into quantitative predictions by quantifying the actual area of the air-water interface (A) during wave breaking, meaning that it also accounts for the surface area of bubbles, sprays and droplets. The time histories of the overall air/water interface area are



a)



b)

FIG. 2. Time history of mean gas concentration in water (a) and of the non-dimensional energy dissipation rate in water (b) for different values of the initial steepness and Reynolds number. The horizontal bars in panel (b) indicate the average dissipation rates during the various phases of the breaking and the time intervals over which the averages are taken.

shown in Fig. 3. The data display increase of the interface area also for the spilling breaking case with $\epsilon = 0.37$ and $Re = 40,000$. However, much more significant increase is observed for the plunging breaking cases with $\epsilon = 0.50$, for which the interface area increases by up to a factor two from the initial value. The data in Fig. 3 and those in Fig. 2b clearly display strong correlation between the air entrainment and the increase in the energy dissipation rate, as already noted by [14].

Various theories have been proposed to explain and parameterize gas exchange processes in air-water systems (e.g., [3]). By appealing to the "surface renewal" theory, [32] proposed that the gas transfer velocity is related to the turbulence energy dissipation rate near the air-water interface, raised to the 1/4 power. Similarly, [12] derived a comparable result by modeling the influence of turbulence patches enhanced by breaking (e.g., [33]). In [13], the theory of [32] was applied to estimate the gas transfer velocity in breaking waves, assuming that the near-surface turbulent dissipation rate is connected to

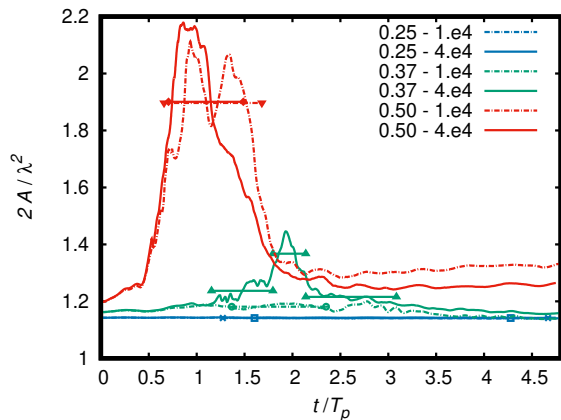


FIG. 3. Time histories of the overall air-water interface area, normalized by the $x - z$ plane projected area ($\lambda^2/2$). The horizontal bars indicate the average values during the various phases of the breaking and the time intervals over which the averages are taken.

the energy dissipation rate in water. The results shown in Fig. 2 indeed corroborate these statements, confirming that the gas transfer rate is strongly correlated with the energy dissipation rate. Quantitative evaluation of the gas transfer rate can be made in terms of the mass flux per unit surface, namely $J = 1/A dq_w/dt$, with q_w defined in equation (2). Following [7], we define the gas transfer velocity as

$$k_L = \frac{1}{A} \frac{dq_w/dt}{(\bar{c}_w - \alpha \bar{c}_a)}, \quad (3)$$

where the mean gas concentrations in the two fluids are used.

The time histories of the gas transfer velocity are shown in Fig. 4. All plots display unnaturally large values in the initial stages owing to the start-up transient. Afterwards, the gas transfer velocity increases significantly with the initial wave steepness and the breaking intensity, which is consistent with what found for the average concentration in Fig. 2a. The data also indicate that for waves with same initial steepness the gas transfer velocity increases when increasing the Reynolds number, hence with the dimensional wavelength, in agreement with the observations of [16]. Comparing the time histories with the results of Fig. 2b and Fig. 3, we further note that the gas transfer velocity attains its peak at about the same time as the energy dissipation rate and the air-water interface area. The fact that k_L , which is evaluated by using the overall air/water interface area, attains its maximum value when A is also maximum, suggests that the increase in the gas flux is much stronger than due to the sole increase of the air/water interface area. In other words, not only does air entrainment widen the interface area through which the gas exchange takes place, but it also enhances the gas transfer velocity by magnifying the velocity gradients occurring around the air/water inter-

face as a consequence of bubble fragmentation processes, as highlighted from the concentration fields in Fig. 1.

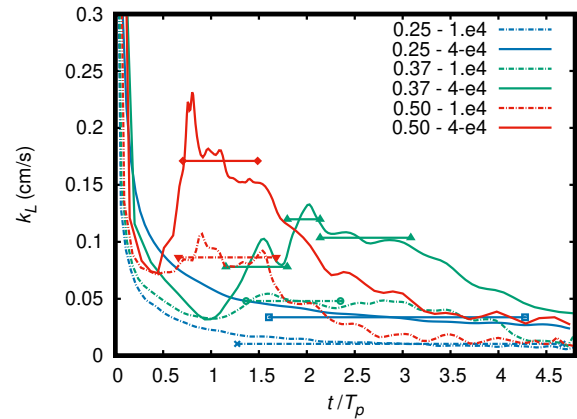


FIG. 4. Time histories of the gas transfer velocity, as defined in (3). The average values computed during the same intervals used for the energy dissipation rates in Fig. 2 are also shown.

It is worth remarking that the estimation of gas transfer velocity, as defined in equation 3, relies on the overall air-water interface area. While this quantity is readily available in numerical simulations, laboratory or field experiments typically estimate k_L using the waterplane area as a surrogate. As shown in Fig. 3, this approximation can be inadequate, particularly for energetic plunging breaking cases, where the interface area can reach up to twice its initial value and more than double the waterplane area, which for the present simulations is $\lambda^2/2$. Numerical simulations thus provide an unprecedented opportunity to accurately evaluate the energy dissipation rate and gas transfer velocity based on the overall interface area. This enables validation of power-law formulas currently in use [13]. The data for the various cases are presented in Fig. 5. Despite noticeable dispersion in the data points, the gas transfer velocity computed using the overall interface area (open symbols) exhibits a clear increasing trend, consistent with the $1/4$ power-law model. Conversely, the velocity estimated using the waterplane area (filled symbols) is slightly higher than that based on the overall interface area for most cases. However, for the two plunging breaking cases, the values based on the waterplane area are nearly double the true values.

In conclusion, this work, for the first time to the authors' knowledge, utilizes a multiphase flow solver to compute the gas transfer velocity in a wave-breaking flow. It highlights the critical role of air entrainment during breaking events in enhancing gas transfer. The study also demonstrates the importance of accounting for the overall air-water interface area to derive accurate estimates of gas transfer velocity—something achievable only with multiphase flow solvers. The computed gas transfer velocities are found to scale with the energy dissipation rate to the power of $1/4$, consistent with theoretical predictions. This scaling is particularly relevant because, at

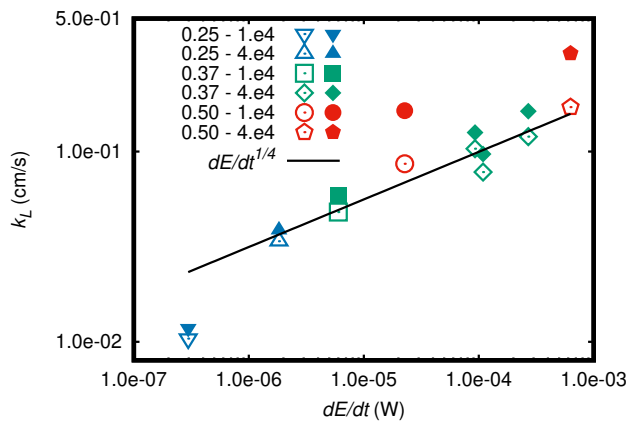


FIG. 5. Gas transfer velocity based on the overall air-water interface (open symbols) and based on the waterplane area (solid symbols), as a function of the respective dissipation rate. The line represents the 1/4 power of the energy dissipation rate.

least for the potential energy component, the dissipation rate can be estimated from free surface measurements. However, estimating the air-water interface area is more complex. A potential approach involves combining the volume flux of air entrained, as suggested in [34], with the bubble size distribution proposed in [35]. It is important to note that this study does not account for the effects of wind, which are expected to significantly influence gas transfer due to wind stress and turbulence. As shown in [36], which focuses on heat transfer, the inclusion of wind introduces additional complexities. This challenging aspect will be addressed in future studies.

ACKNOWLEDGMENTS

We acknowledge that the results reported in this paper have been achieved using the EuroHPC Research Infrastructure resource LEONARDO based at CINECA, Casalecchio di Reno, Italy.

-
- [1] A. J. Watson, U. Schuster, J. D. Shutler, T. Holding, I. G. Ashton, Landschützer, D. K. Woolf, and L. Goddijn-Murphy, Revised estimates of ocean-atmosphere CO_2 flux are consistent with ocean carbon inventory, *Nat. Commun.* **11** (2020).
 - [2] P. Friedlingstein, M. O’sullivan, M. W. Jones, R. M. Andrew, J. Hauck, A. Olsen, G. P. Peters, W. Peters, J. Pongratz, S. Sitch, *et al.*, Global carbon budget 2020, *Earth Syst. Sci. Data Discuss.* **2020**, 1 (2020).
 - [3] B. Jähne and H. Haußecker, Air-water gas exchange, *Annu. Rev. Fluid Mech.* **30**, 443 (1998).
 - [4] G. H. Jirka, H. Herlina, and A. Niepelt, Gas transfer at the air–water interface: experiments with different turbulence forcing mechanisms, *Exp. Fluids* **49**, 319 (2010).
 - [5] D. Deising, D. Bothe, and H. Marschall, Direct numerical simulation of mass transfer in bubbly flows, *Comput. Fluids* **172**, 524 (2018).
 - [6] L. Deike, Mass transfer at the ocean–atmosphere interface: the role of wave breaking, droplets, and bubbles, *Annu. Rev. Fluid Mech.* **54**, 191 (2022).
 - [7] R. Wanninkhof, W. E. Asher, D. T. Ho, C. Sweeney, and W. R. McGillis, Advances in quantifying air–sea gas exchange and environmental forcing, *Annu. Rev. Mar. Sci.* **1**, 213 (2009).
 - [8] W. E. Asher and T. M. Litchendorf, Visualizing near-surface concentration fluctuations using laser-induced fluorescence, *Exp. Fluids* **46**, 243 (2009).
 - [9] C. R. Chu and G. H. Jirka, Wind and stream flow induced reattachment, *Environ. Eng.* **129**, 1129 (2003).
 - [10] Herlina and G. H. Jirka, Application of lif to investigate gas transfer near the air–water interface in a grid-stirred tank, *Exp. Fluids* **37**, 341 (2004).
 - [11] C. S. Garbe, A. Rutgeresson, J. Boutin, G. de Leeuw, B. Delille, C. W. Fairall, N. Gruber, J. Hare, D. T. Ho, N. P. D. Johnson, Martin T, H. Pettersson, S. E. T. W.-T. Piskozub, Jacek, B. Ward, D. K. Woolf, and C. J. Zappa, Ocean–atmosphere interactions of gases and particles (Springer Earth System Sciences, 2014) Chap. Transfer Across the Air–Sea Interface.
 - [12] S. A. Kitaigorodskii, On the fluid dynamical theory of turbulent gas transfer across an air–sea interface in presence of breaking wind–waves, *J. Phys. Oceanogr.* **14**, 960 (1984).
 - [13] L. Shuiqing and Z. Dongliang, Gas transfer velocity in the presence of wave breaking, *TELLUS B.* **68**, 27034 (2016).
 - [14] A. Iafrazi, Energy dissipation mechanisms in wave breaking processes: spilling and highly aerated plunging breaking events, *J. Geophys. Res.* **116**, C07024 (2011).
 - [15] R. H. Stanley, W. J. Jenkins, D. E. Lott III, and S. C. Doney, Noble gas constraints on air–sea gas exchange and bubble fluxes, *J. Geophys. Res.* **114**, C11020 (2009).
 - [16] S. Li, A. V. Babanin, F. Qiao, D. Dai, S. Jiang, and C. Guan, Laboratory experiments on CO_2 gas exchange with wave breaking, *J. Phys. Oceanogr.* **51**, 3105 (2021).
 - [17] P. K. Farsoiyya, S. Popinet, and L. Deike, Bubble-mediated transfer of dilute gas in turbulence, *J. Fluid Mech.* **920**, A34 (2021).
 - [18] S. Mirjalili, S. S. Jain, and A. Mani, A computational model for interfacial heat and mass transfer in two-phase flows using a phase field method, *Int. J. Heat Mass Transf.* **197**, 123326 (2022).
 - [19] L. Deike, S. Popinet, and W. K. Melville, Capillary effects on wave breaking, *J. Fluid Mech.* **769**, 541 (2015).
 - [20] S. Di Giorgio, S. Pirozzoli, and A. Iafrazi, On coherent vortical structures in wave breaking, *J. Fluid Mech.* **947**, A44 (2022).
 - [21] G. D. Weymouth and D. K.-P. Yue, Conservative volume-of-fluid method for free-surface simulations on cartesian grids, *J. Comput. Phys.* **229**, 2853 (2010).
 - [22] S. Di Giorgio, S. Pirozzoli, and A. Iafrazi, Evaluation of advection schemes and surface tension model for algebraic and geometric vof multiphase flow solvers, *J. Comput. Phys.* **499**, 112717 (2024).

- [23] G. Standart, The mass, momentum and energy equations for heterogeneous flow systems, *Chem. Eng. Sci.* **19**, 227 (1964).
- [24] Y. Haroun, D. Legendre, and L. Raynal, Volume of fluid method for interfacial reactive mass transfer: Application to stable liquid film, *Chem. Eng. Sci.* **65**, 2896 (2010).
- [25] D. Bothe and S. Fleckenstein, A volume-of-fluid-based method for mass transfer processes at fluid particles, *Chem. Eng. Sci.* **101**, 283 (2013).
- [26] R. Sander, Compilation of henry's law constants (version 5.0. 0) for water as solvent, *Atmos. Chem. Phys.* **23**, 10901 (2023).
- [27] D. Deising, H. Marschall, and D. Bothe, A unified single-field model framework for volume-of-fluid simulations of interfacial species transfer applied to bubbly flows, *Chem. Eng. Sci.* **139**, 173 (2016).
- [28] S. Pirozzoli, S. Di Giorgio, and A. Iafrati, On algebraic tvd-vof methods for tracking material interfaces, *Comput. Fluids* **189**, 73 (2019).
- [29] A. Iafrati, Numerical study of the effects of the breaking intensity on wave breaking flows, *J. Fluid Mech.* **622**, 371 (2009).
- [30] L. Memery and L. Merlivat, Modelling of gas flux through bubbles at the air-water interface, *TELLUS B.* **37**, 272 (1985).
- [31] W. E. Asher, L. Karle, B. Higgins, and P. Farley, The influence of bubble plumes on air-seawater gas transfer velocity, *J. Geophys. Res.* **101 - C5**, 12027 (1996).
- [32] J. Lamont and D. Scott, A eddy cell model of mass transfer into the surface of a turbulent liquid, *AIChE J.* **16**, 513 (1970).
- [33] C. J. Zappa, W. R. McGillis, P. A. Raymond, J. B. Edson, E. J. Hinst, H. J. Zemmeling, J. W. H. Dacey, and D. T. Ho, Environmental turbulent mixing controls on air-water gas exchange in marine and aquatic systems, *Geophys. Res. Lett.* **34**, L10601 (2007).
- [34] L. Deike and W. Melville, Gas transfer by breaking waves, *Geophys. Res. Lett.* **45**, 10482 (2018).
- [35] G. Deane and M. Stokes, Scale dependence of bubble creation mechanisms in breaking waves, *Nature* **418**, 839 (2002).
- [36] M. Lu, Z. Yang, G. He, and L. Shen, Numerical investigation on the heat transfer in wind turbulence over breaking waves, *Phys. Rev. Fluids* **9**, 084606 (2024).